Atmospheric Environment 44 (2010) 1043–1053

Contents lists available at ScienceDirect

Atmospheric Environment

journal homepage: www.elsevier.com/locate/atmosenv

Dust emissions created by low-level rotary-winged aircraft flight over desert surfaces

J.A. Gillies*, V. Etyemezian, H. Kuhns, J.D. McAlpine, J. King, S. Uppapalli, G. Nikolich, J. Engelbrecht

Desert Research Institute, Division of Atmospheric Sciences, 2215 Raggio Parkway, Reno, NV 89512, United States

ARTICLE INFO

Article history:
Received 25 August 2009
Received in revised form
11 December 2009
Accepted 16 December 2009

Keywords:
Rotary-winged aircraft
Dust emissions
Military testing and training activities

ABSTRACT

There is a dearth of information on dust emissions from sources that are unique to U.S. Department of Defense testing and training activities. Dust emissions of PM_{10} and $PM_{2.5}$ from low-level rotary-winged aircraft travelling (rotor-blade ≈7 m above ground level) over two types of desert surfaces (i.e., relatively undisturbed desert pavement and disturbed desert soil surface) were characterized at the Yuma Proving Ground (Yuma, AZ) in May 2007. Fugitive emissions are created by the shear stress of the outflow of high speed air created by the rotor-blade. The strength of the emissions was observed to scale primarily as a function of forward travel speed of the aircraft. Speed affects dust emissions in two ways: 1) as speed increases, peak shear stress at the soil surface was observed to decline proportionally, and 2) as the helicopter's forward speed increases its residence time over any location on the surface diminishes, so the time the downward rotor-generated flow is acting upon that surface must also decrease. The state of the surface over which the travel occurs also affects the scale of the emissions. The disturbed desert test surface produced approximately an order of magnitude greater emission than the undisturbed surface. Based on the measured emission rates for the test aircraft and the established scaling relationships, a rotary-winged aircraft similar to the test aircraft traveling 30 km h^{-1} over the disturbed surface would need to travel 4 km to produce emissions equivalent to one kilometer of travel by a light wheeled military vehicle also traveling at 30 km h^{-1} on an unpaved road. As rotary-winged aircraft activity is substantially less than that of off-road vehicle military testing and training activities it is likely that this source is small compared to emissions created by ground-based vehicle movements.

1. Introduction

A multi-year effort has been underway to understand the contributions of military testing and training activities to regional particulate matter, particularly mineral dust particles of aerodynamic diameter ≤10 μm (PM_{10}) and aerodynamic diameter ≤2.5 μm ($PM_{2.5}$), in the western U.S. As part of this effort, a study was undertaken to measure mineral dust emissions created by a rotary-winged aircraft (UH-1 Huey/Bell 212) flying at a low-level (rotor-blade ≈7 m above ground level, AGL) over two different desert surface types at the Yuma Proving Ground (YPG), Yuma AZ (Fig. 1). Contributions of particulate matter to the atmosphere by rotary-winged aircraft are not addressed in conventional air emissions information resources such as the U.S. EPA's (1996) "AP-42, Compilation of Air Pollutant Emission Factors, Vol. 1: Stationary Point and Area Sources". Nor is there much information available in the literature that relates helicopter operating parameters to dust generation by rotor-created wakes that interact with a surface that is susceptible to dust emission. Cowherd (2007) reported that measured dust concentrations in plumes raised by five different rotary-winged and a tilt-rotor aircraft performing a hover-taxi maneuver scaled with the helicopter mass divided by area swept by the rotor (i.e., A (m^2) = πR^2, where R = length of rotor-blade, and termed the disk loading) for a disturbed desert surface at the YPG. He also observed that as aircraft size increased, the particle size of entrained dust converged, but the sand-sized particles entrained by the rotor-wash increased indicating that the stronger downwash and outflow for larger aircraft is more effective in entraining larger particles into the dust cloud.

To provide data on the potential magnitude of dust emissions caused by this military source, a field measurement campaign was undertaken from 21–25 May, 2007, at the YPG. Emissions of dust created by a low-flying rotary-winged aircraft were measured for helicopter passes over two different surfaces, which represented a desert pavement with minimal disturbance and an area within the YPG that is used for drop-zone testing (parachute-aided landings of military matériel and personnel) and can be considered

* Corresponding author.
E-mail address: Jack.Gillies@dri.edu (J.A. Gillies).

1352-2310/$ – see front matter © 2009 Elsevier Ltd. All rights reserved.
doi:10.1016/j.atmosenv.2009.12.018

Fig. 1. The test aircraft creating dust emissions in the designated flight path at Site 2, Yuma Proving Ground.

a disturbed desert surface. Both test locations were flat with large upwind fetches relative to the defined flight path line.

The emissions of dust generated by the low-level flight of the aircraft were measured downwind of the flight path at distances between 100 m and 145 m using a three tower measurement system similar to that used by Gillies et al. (1999, 2005, 2007a) and Kuhns et al. (in press) to measure dust emissions from wheeled and tracked military vehicles and artillery backblast. Meteorological variables were also collected including wind speed profiles, point measurements of three-dimensional wind vectors, wind direction, and surface shear stress. In addition to the dust flux measurements, surface dust emission potential measurements were made using the Portable In-Situ Wind Erosion Laboratory (PI-SWERL) described by Etyemezian et al. (2007), Sweeney et al. (2008), and Kavouras et al. (2009). These measurements provide a means to compare how the surface conditions affect the strength of the dust emissions.

The overall purpose of the study was to examine the relationship between aircraft operating parameters, the characteristics of the surfaces, and the measured dust emissions. This opportunity was also used to collect a limited data set on dust emissions that result from helicopter take-off and landing in addition to those that result from low-level flight.

2. Background

Sources of particulate matter (PM) dust associated with some U.S. Department of Defense (DoD) testing and training activities have equivalency or at least similarity to source types encountered in the civilian environment. For example, Gillies et al. (2005) and Moosmüller et al. (2005) have characterized the mass emissions of PM_{10} (PM with aerodynamic diameter $\leq$10 μm) and incremental visibility impairment for wheeled military and civilian vehicles traveling on an unpaved road. Kuhns et al. (in press) examined dust emissions on unpaved surfaces for both wheeled and tracked military vehicles and reported that the strength of the emissions are controlled by a vehicle's momentum (weight $\times$speed) and by the emissive properties of the unpaved travel surface. There are however, other sources of dust emissions that are unique to DoD activities for which the PM emission factors are entirely uncharacterized. Recent work by Gillies et al. (2007a) has provided new information on unique DoD sources of mineral particles emitted to the atmosphere, such as artillery backblast.

The emissions of dust from rotary-winged aircraft were identified as a potentially important source category for PM originating from military testing or training activities. The ability to estimate contributions from this source was severely hampered by a lack of data and a limited understanding of the interaction of rotary-winged aircraft-created wakes with surfaces that have the potential to emit dust. The research reported here is part of a larger study supported by the Strategic Environmental Research and Development Program (SERDP) to refine or develop new understanding of the contributions of airborne PM that can be generated from unique DoD sources, such as rotary-winged aircraft. A brief introduction to rotary-winged aircraft operation and wake development (rotor downwash) is provided.

A rotary-winged aircraft controls its forward travel speed by changing the pitch of the rotor, which creates an uneven distribution of the lift force, with more downward thrust at the rear and less downward thrust at the front, which causes the main rotor mass to tilt forward. The revolutions per unit time for the blades are relatively invariant once take-off has occurred. During near surface flight operations the ground effect flow pattern created by the aircraft can be classified into different flow regimes: jet wake, recirculation, ground vortex, and trailing sweep (Curtiss et al., 1984, 1987; Ganesh and Komerath, 2004a,b, 2006). The flow regime that develops is dependent upon the advance ratio of the helicopter and height of the rotor above the ground. Advance ratio, μ, is defined as follows:

$$\mu = \frac{V}{\Omega R} \tag{1}$$

where V is forward speed of the helicopter multiplied by the cosine of the ambient wind direction (m s^{-1}) with respect to travel direction, Ω is the rotor angular velocity (m s^{-1}, constant for a given aircraft), and R is the rotor radius (m). For details relating to flow regime physics the reader is referred to Curtiss et al. (1984) and Brown and Whitehouse (2004). The strength of dust emissions could be affected by the type of flow regime created by the aircraft as they have different flow features that interact with the surface.

Under all flow regimes, a feature of the ground effect wake is asymmetry of the vortex on different sides of the helicopter. The ground vortex on the advancing side of the rotor (i.e., blade moving in the forward travel direction) is stronger and more established while it is weaker and more unstable on the retreating side of the rotor due to the rotor-blade trimming (Brown and Whitehouse, 2004).

The flow regime conditions can be described as follows:

2.1. Jet-wake

This regime occurs with low free-stream wind speeds opposing the induced ground jet of the wake, so no vortex forms within the wake. The flow is like an impinging jet, impacting the surface below the rotor and fanning out radially.

2.2. Recirculation

This regime is characterized by a semi-permanent large vortex in front of the helicopter. This flow regime is also characterized by a distinct ground jet that expands beyond the length of the rotor to a separation point. At this point the jet turns vertically and wraps back around towards the rotor due to forcing by the free-stream wind.

2.3. Ground vortex

This flow regime is characterized by a contracted horseshoe-shaped vortex positioned under the rotor. The ground vortex flow

regime is typically characterized by a more stable flow structure than the recirculation regime.

2.4. Trailing sweep

In this flow regime the wake tends to flatten and take the characteristics of a fixed-wing wake, with two counter-rotating "wingtip" vortices extending downwind of the rotor edges. The bottom edge of the vortices can be in contact with the surface and hence low enough to potentially induce dust entrainment.

Schematic representations and images of the aircraft in these ground effects are illustrated in Fig. 2.

As rotor angular velocity and radius are important factors in the development of flow regime character, it needs to be noted that the data collected as part of this study are representative of the helicopter being tested (or one of similar rotor characteristics). Rotor size and angular velocity will scale principally with the weight of the aircraft and also be complicated, for purposes of comparison among different types of helicopters, by the configuration of rotors (i.e., tail rotor or tandem rotor designs).

3. Methods

To measure the dust emissions and ambient wind conditions three towers were set up perpendicular to a section of desert surface delineated with traffic cones. Each section was ≈200 m long and ≈50 m wide. The three towers were all downwind of the flight corridor at distances of 100 m and 145 m for Sites 1 and 2, respectively. An image of the tower monitoring system and a schematic of the instrument positions are shown in Fig. 3.

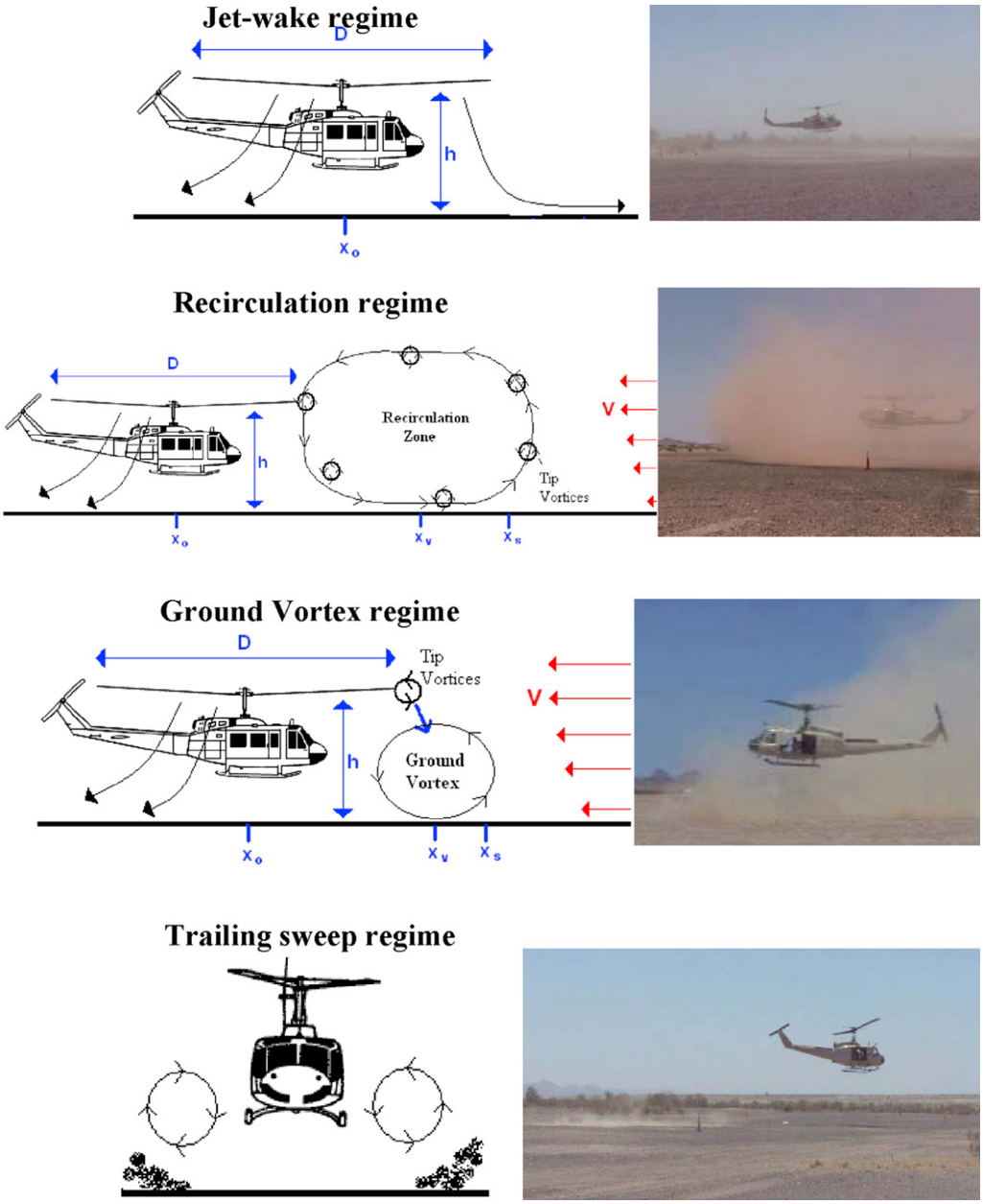

Fig. 2. Schematic diagrams of rotor wake flow regimes and images of the aircraft for these ground effect states taken at the Yuma Proving Ground. Arrows beside images show direction the ambient winds are approaching from with respect to the aircraft (after McAlpine et al., submitted for publication).

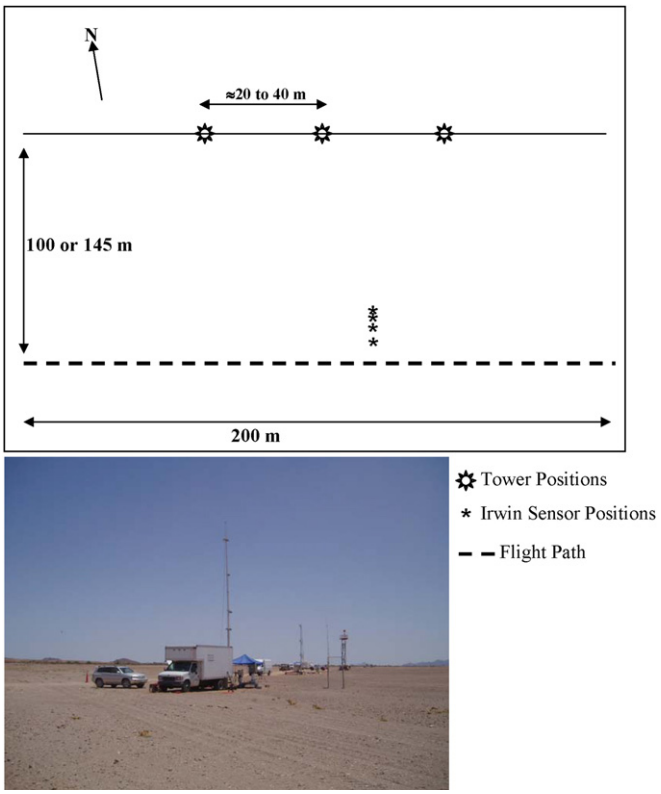

Fig. 3. Schematic diagram of the test area and instrumentation layout set up to measure dust emissions generated by the helicopter. The three visible towers comprise the DRI flux tower system. Additional instrumentation consisting of optical remote sensing instruments is also shown.

The center tower was instrumented with ten real-time dust monitors (i.e., DustTrak Model 8520, TSI Inc., St. Paul, MN): five configured to measure PM_{10} and five configured to measure $PM_{2.5}$. On the center tower, the dust monitors were spaced logarithmically in the vertical direction at heights AGL of 1.67 m, 2.64 m, 3.98 m, 6.47 m, and 9.12 m. The DustTrak is a portable, battery-operated, laser-photometer that uses light scattering technology to determine mass concentration in real-time and has been used in other field studies measuring dust emissions (e.g., Gillies and Berkofsky, 2004; Gillies et al., 2005, 2007a) and particulate emissions from mobile sources (e.g., Moosmüller et al., 2001a,b).

Wind speed was measured using cup anemometers (RM Young Wind Sentry) at the same height above the ground as the dust measurements. Wind direction was measured at 9.12 m AGL with a wind vane (RM Young Wind Sentry). Three-dimensional wind vectors associated with the rotor-wash were measured with a sonic anemometer at 1.5 m AGL at one position on the flight path, approximately 7.3 m from the centerline where the outer edge of the rotor-blade was expected to pass as the helicopter made its low-level pass down the flight corridor.

The two towers on either side of the center tower held PM_{10} dust monitors (also TSI Model 8520 DustTraks) at 2.74 m, 5.1 m, 6.9 m, and 14.2 m and $PM_{2.5}$ dust monitors at 2.74 m and 5.1 m AGL. These towers were collinear with the center tower and placed on opposite sides of the center tower at distances of 29 m and 20 m at Site 1, and 34 m and 41 m at Site 2. The background levels of PM_{10} and $PM_{2.5}$ at each measurement level and position were estimated from 15 one second concentration measurements prior to the arrival of the aircraft at the test site. These 15 sec average concentration values were subsequently subtracted from each one second measurement during the time the dust plume impacted the monitors.

The mass of particulate matter produced by the part of the dust plume that passed the instrument array can be calculated as:

$$\text{Total Mass of particulate(kg)} = \sum_{1}^{14} C \times \text{WS} \times T \times A \times \text{cosine WD} \quad (2)$$

where: C = background subtracted particulate matter concentration (kg m^{-3}); WS = wind speed (m s^{-1}); T = duration of plume impact (s); A = area of plane (m^2, represented by an individual dust monitor); WD = wind direction (degrees).

The summation represents the 14 defined planes in the instrument array (Fig. 4).

This calculation makes the following assumptions (Fig. 4): 1) the point concentration measurement of PM_{10} (or $PM_{2.5}$ for the center tower) is constant throughout an area defined by the length dimensions equal to one-half the horizontal distance between the two closest towers and extending that same distance outward from the two end towers and a height of one-half the distance between two dust monitors in the vertical on the same tower; 2) the vertical extent of the area defined for the highest sensors is assumed to extend in the vertical the same distance as one-half the distance to the next lowest sensor; 3) the wind speed is assumed to be constant in a horizontal plane defined for each anemometer that extends in the vertical to a point that is one-half the distance between two anemometers in the vertical on the central tower that extends horizontally to the entire defined length of the instrument array; and 4) winds approaching the instrument array at an angle $\geq 45^{\circ}$ from the perpendicular invalidate the measurements associated with a flight pass.

To link the light scattering measurements made with the DustTrak instrument with gravimetrically-derived concentration measurements, a comparison was made between DustTrak measurements and filter-based methods using a resuspension technique (Chow et al., 1994) in the laboratory. The details of this procedure are given in Kuhns et al. (in press). All reported PM concentrations and fluxes have been converted to gravimetric equivalent measurements based on the laboratory-established relationship.

In addition to the dust and meteorological sensors, four Irwin sensors (Irwin, 1980) were emplaced in the ground along an ≈19 m long transect normal to the flight path, beginning at a location 10 m from the center of the flight line. The four Irwin sensors were separated in decreasing distance from the edge of where the rotor-wash was expected to become directed laterally (i.e., 10 m, 15, m, 17.5 m, and 18.75 m) and sweep across the surface creating a horizontal shear stress. Irwin sensors have been previously used to measure surface shear stress generated by atmospheric boundary-layer winds (Gillies et al., 2006, 2007b). The purpose of these measurements is to relate helicopter operating conditions with the surface winds they generate and the associated dust emission strength.

To create the dust emissions the helicopter pilot was requested to make low-level passes traveling in the direction along the defined flight path corridor opposite to the prevailing wind. The target forward travel speed range was 15 km h^{-1} (4 m s^{-1}) to 60 km h^{-1} (17 m s^{-1}). For each pass the target speed was increased incrementally from the minimum to maximum and then decreased incrementally from maximum to minimum. Actual forward travel speeds were resolved using video imagery recorded for each flight pass. The dust plume was allowed to completely pass by the instruments before the next flight pass was requested.

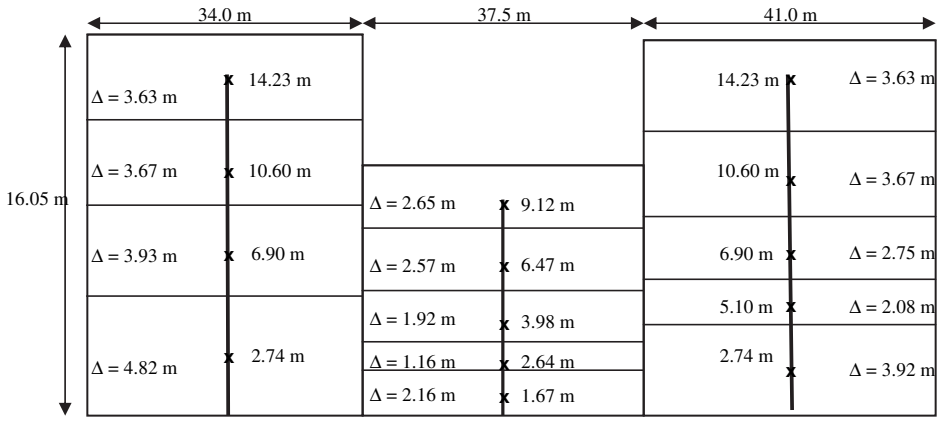

Fig. 4. Schematic diagram of the instrument placements and 14 defined flux planes used to calculate the emission flux of PM_{10} and $PM_{2.5}$ created by the aircraft.

As a means to compare the emission potential of different surface types that could be impacted by low-level helicopter passes, in the absence of tower-based measurements of dust flux, the PI-SWERL instrument (Etyemezian et al., 2007; Sweeney et al., 2008; Kavouras et al., 2009) was used to collect data on particulate matter emission potential driven by aerodynamic shear stress imparted to the surface. The PI-SWERL is being used increasingly as a primary tool to evaluate windblown dust emissions from natural and artificial soil surfaces (Fig. 5) and relating dust emission strength to, for example, soil parameters and salt content (Etyemezian et al., 2007; Kavouras et al., 2009; Goossens and Buck, 2009; King et al., submitted for publication). Unlike large (10 m or longer) field wind tunnels, the PI-SWERL does not meet many of the scaling criteria that are theoretically required for realistic simulations of aeolian sediment transport processes. However, recent research, and comparison of measured emission fluxes with those derived from large portable field wind tunnel testing indicate that the PI-SWERL does provide a reliable measure of windblown dust emission potential (Sweeney et al., 2008).

The PI-SWERL is a cylindrical chamber ($D = 30$ cm, $H = 20$ cm) that has an open end which is placed over the soil surface to be tested. Ventilation of the PI-SWERL chamber is accomplished by a DC blower (AMETEK, Mini-Jammer) and monitored by a mass flow meter (TSI, Model 42350101). Filtered air that is introduced by the blower, mixes with the air in the chamber and the flow is exhausted through a port (diameter = 5.0 cm) at the top of the chamber. Dust suspension within the chamber is induced by a rotating, flat annular ring (inner diameter = 0.16 m, outer diameter = 0.25 m). Once the measurement cycle is initiated, one second concentrations of PM_{10} are measured by a DustTrak (TSI, Inc., Model 8520).

The PM_{10} concentration (C, μg m^{-3}) at the outlet of the instrument is recorded at 1 Hz while a blower vents clean air through the PI-SWERL at a constant rate (F, m^3 s^{-1}) and the emission flux (μg m^{-2} s^{-1}) or amount of PM_{10} produced per area per second is calculated as:

$$E_{i,\mathrm{cum}} = \frac{\sum_{\mathrm{begin},1}^{\mathrm{end},i} C \times F}{t_{\mathrm{end},i} - t_{\mathrm{begin},i}} \Big/ A_{\mathrm{eff}} \quad (3)$$

where the summation occurs over every one second measurement during level i, beginning at $t_{\mathrm{begin},i}$ and ending at $t_{\mathrm{end},i}$, with t as integer seconds. The measured dust concentration and flow rate are converted to an emission flux by the effective area of the PI-SWERL, A_{eff} which is 0.026 m^2. The PI-SWERL tests measure the potential fugitive PM_{10} dust emissions from the surface at different equivalent wind speeds up to a wind speed of roughly 30 m s^{-1} at 2 m AGL.

PI-SWERL tests were conducted at each site before and after the helicopter passes. At each site multiple PI-SWERL tests were conducted on a parallel transect directly below where the helicopter flew. At site 1, 11 tests were conducted with eight before the helicopter passes and three tests after the passes were completed. Seventeen PI-SWERL tests were conducted at site 2.

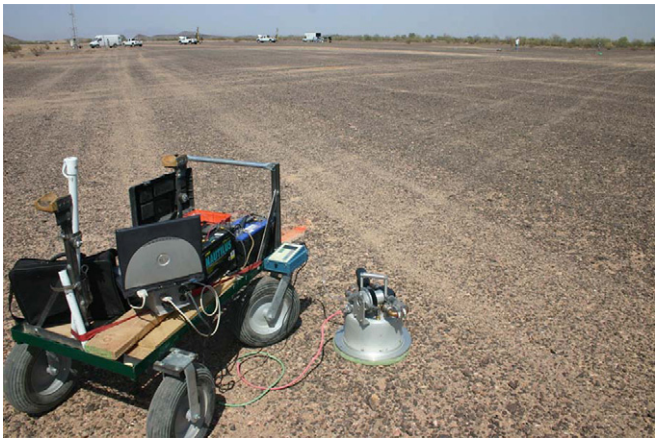

Fig. 5. The DRI PI-SWERL deployed to measure potential dust emissions at Site 1, YPG.

4. Results

The flight maneuvers made by the helicopter at each of the two test sites are summarized as followed: 1) site 1, 36 passes spanning the target forward travel speed range and four landing and take-offs; 2) site 2, 37 passes covering the target forward travel speed range. Based on analysis of the video imaging of each flight pass the average height of the rotor-blade AGL was 7.1 m (±0.5 m). The type of flow regimes associated with the flight passes were calculated based on advance ratio estimates (Table 1). The most commonly occurring flow regime was ground vortex (39% occurrence), followed by re-circulating (30% occurrence) and trailing sweep (21%), no jet wakes were observed. The remaining 16% were categorized as transitional (13%) or un-defined (3%).

4.1. Dust emissions

An accounting of the reliability of the acquired dust emission data for subsequent analysis is provided in Table 2. Reliability for

Table 1
Dust emission test conditions and measurement parameters for the rotary-winged aircraft flights at Sites 1 and 2, YPG. Upper table entries are for PM_{10} and the lower entries for $PM_{2.5}$.

Site	Target forward travel speed (km h^{-1})	Average forward travel speed (km h^{-1})	Standard deviation of forward travel speed (km h^{-1})	Average advance ratio	Standard deviation of advance ratio	Average per tower total emissions[a] (kg of PM_{10} per flight pass)	Standard deviation of total emissions[a] (kg of PM_{10} per flight pass)	Average per tower unit emissions per m width (g of PM_{10} m^{-1})	Number of flight passes
1	15	19.4	1.4	0.012	0.006	0.266	0.336	0.019	14
1	30	30.3	11.1	0.029	0.029	0.070	0.117	0.005	13
1	60	58.3	6.8	0.066	0.012	0.065	0.059	0.005	15
2	15	19.1	1.4	0.025	0.007	15.717	10.541	0.301	27
2	25	26.6	1.2	0.035	0.004	6.202	6.062	0.119	24
2	35	35.6	2.2	0.045	0.006	3.955	3.794	0.076	25
2	45	44.9	3.6	0.055	0.008	0.683	0.792	0.013	28
2	60	58.5	0.7	0.061	0.002	0.071	0.071	0.001	3
Site	Target forward travel speed (km h^{-1})	Average forward travel speed (km h^{-1})	Standard deviation of forward travel speed (km h^{-1})	Average advance ratio	Standard deviation of advance ratio	Average per tower total emissions[a] (kg of $PM_{2.5}$ per flight pass)	Standard deviation of total emissions[a] (kg of $PM_{2.5}$ per flight pass)	Average Per Tower Unit Emissions per m width (g of $PM_{2.5}$ m^{-1})	Number of Flight Passes
1	15	19.4	1.4	0.012	0.006	N/A			
1	30	30.3	11.1	0.029	0.029	N/A			
1	60	58.3	6.8	0.066	0.012	N/A			
2	15	19.1	1.4	0.025	0.007	1.641	1.590	0.031	27
2	25	26.6	1.2	0.035	0.004	0.497	0.451	0.010	24
2	35	35.6	2.2	0.045	0.006	0.404	0.393	0.008	25
2	45	44.9	3.6	0.055	0.008	0.049	0.062	0.001	28
2	60	58.5	0.7	0.061	0.002	N/A			

[a] Based on total flux for each of the three towers.

these data is defined in terms of data acquisition faults, angle of wind approach to the instrument array, particulate matter concentrations in exceedance of the instrument limits (i.e., $\geq 1.5 \times 10^5$ μg m^{-3}), and for minor extrapolation of dust concentration when less than 90% or between 70% and 80% of the instruments were operating (individual instrument failure sometimes occurred during testing, which could not be rectified in the time between passes). Reasons for a failure to observe emissions were attributed to variable winds that caused the plume to miss the instrument array, or because winds dropped to near-zero speed creating a plume that dispersed mostly due to thermal instabilities, which is not amenable to a standard horizontal flux calculation.

The duration that the helicopter-generated plumes impacted the towers ranged from 7 s to 107 s at site 1, and 13 s to 180 s at site 2. These times depended primarily on wind speed and wind direction in the ambient boundary-layer wind flow.

Table 2
Report on of the reliability of the acquired dust emission data.

Date	5/21/2007	5/25/2007
Total Flight Passes	36	37
Error Types:		
1) Data acquisition faults	0	0
2) Wind Approach Angle >45°	5 (14%)	1 (3%)
3) Maximum of any DustTrak >150,000 μg m^{-3}	0	0
4) Number invalid plume events due to both wind direction or maximum PM concentration at highest positioned DustTrak >150,000 μg m^{-3}	0	0
5) PM_{10} inferred from minor extrapolation with 90–100% of DustTraks recording, and 100% of meteorological instruments recording	30 (83%)	36 (97%)
6) 70–80% of DTs recording plume, 100% meteorological instruments working	1	(3%)
Average of Top DT>1000 μg m^{-3} (caution, not error)	Tower 1, 0 events Tower 2, 1 event Tower 3, 1 event	Tower 1, 17 events Tower 2, 19 events Tower 3, 9 events

Peak concentrations of $PM_{2.5}$ measured (with the DustTrak sensors) at the towers associated with the dust plumes ranged from 1285 μg m^{-3} to 9925 μg m^{-3} at site 1. Peak concentrations of PM_{10} at site 1 ranged from 6046 μg m^{-3} to 38,860 μg m^{-3}. Background ambient concentrations between helicopter passes ranged between 24 μg m^{-3} and 108 μg m^{-3} for $PM_{2.5}$ and between 55 μg m^{-3} and 499 μg m^{-3} for PM_{10}.

At site 2, peak concentrations of $PM_{2.5}$ measured at the towers associated with the dust plumes ranged from 924 μg m^{-3} to 5874 μg m^{-3}. Peak concentrations of PM_{10} at site 2 ranged from 33,147 μg m^{-3} to 53,170 μg m^{-3}. Background ambient concentrations between helicopter passes ranged between 19 μg m^{-3} and 139 μg m^{-3} $PM_{2.5}$ and between 40 μg m^{-3} and 205 μg m^{-3} for PM_{10}. These background concentration measurements represent average 15 s concentrations (measured at 1 Hz) prior to the arrival of dust plumes.

The 1 s dust concentration data at each of the three towers at multiple heights can be combined with the wind speed and direction data to provide an estimate of how much dust passed through the tower-defined flux plane for each dust plume raised by the helicopter traveling down the flight line i.e., Eq. (2). It should be noted that the actual amounts of dust will be greater than reported here as the defined flux plane does not capture the entire vertical scale of the plumes. The calculation of how many kilograms of dust are passing by the defined flux plane as a function of target and average forward travel speed of the helicopter (determined from individual flight pass video images) are provided in Table 1. The average emissions per meter width (g m^{-1}) of the defined flux plane for both particle sizes are also provided. These latter estimates could form the basis of an emission factor for this type of rotary-winged aircraft flying close to an emissive surface similar to those that are representative of this study.

Clearly, site 2, the disturbed desert soil generates much higher PM_{10} dust emissions for the same helicopter traveling above the ground at the same height and over a similar range of speeds. For the same forward travel speeds of ≈15 km h^{-1} and ≈30 km h^{-1} the emissions increase at site 2 by approximately 60 and 72 times,

respectively. This indicates that disturbance of the soil can have a dramatic impact on the strength of the dust emissions as these two sites are essentially the same surface separated by less than 1000 m from each other, but site 2 has been mechanically disturbed at some time in the past to facilitate its use as a drop-zone. This disturbance has removed the desert pavement and mixed the upper soil horizons. The emissions of $PM_{2.5}$ (Table 1) are approximately 9% (±2%) of the PM_{10}, which is likely dependent, in part, on soil textural and aggregate size properties that change depending on geographic location. It should be noted that the $PM_{2.5}$ emissions are based on fewer measured point concentrations and use the average $PM_{2.5}$:PM_{10} mass concentration ratio to extrapolate concentrations of $PM_{2.5}$ where sensors for this particle size range are missing in the array. This occurs only on the two towers on either side of the center tower. Due to instrument difficulties, adequate data were not available for $PM_{2.5}$ emission calculations at site 1.

The effect of forward travel speed and advance ratio of the aircraft on dust emissions is also evident in the data presented in Table 1. The mean total mass of PM_{10} passing through the array Eq. (2) is plotted as a function of forward travel speed for sites 1 and 2 in Fig. 6 and advance ratio in Fig. 7 (error bars represent standard deviations of the mean values). These two figures show that the mass of PM_{10} emitted from the surface decreases exponentially with increasing forward travel speed and advance ratio. In the larger data set for site 2, forward travel speed seems to be more correlated with emissions than advance ratio, suggesting for these tests forward travel speed is a better predictor for estimating dust emissions.

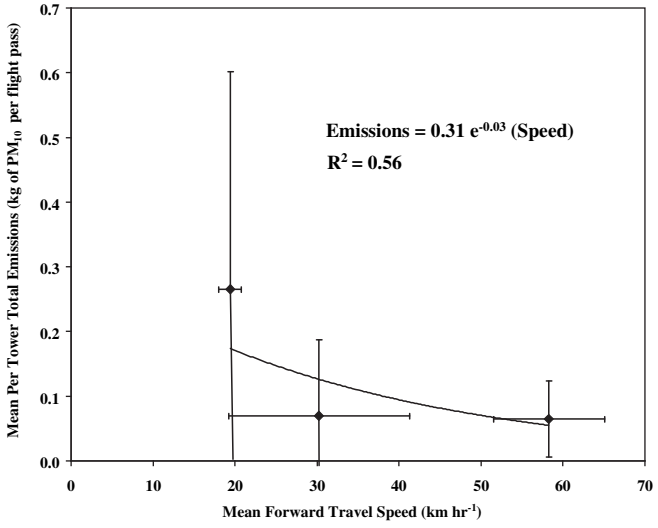

Fig. 6. Emissions of PM_{10} as a function of forward travel speed for Sites 1 and 2, YPG. Error bars represent the standard deviation of the measurement.

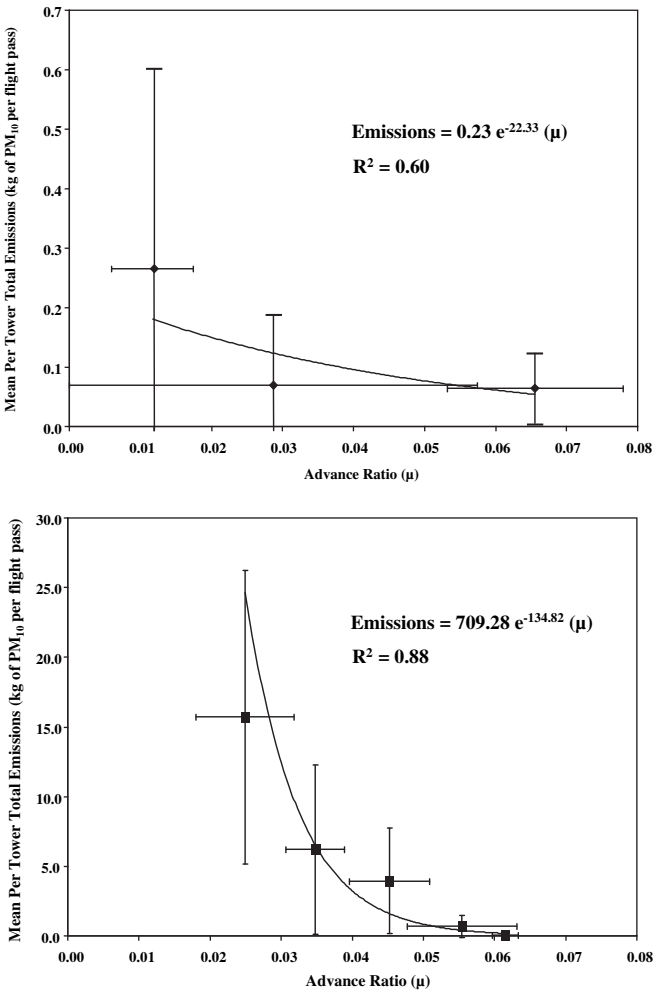

Fig. 7. Emissions of PM_{10} as a function of advance ratio (μ) for Sites 1 and 2, YPG. Error bars represent the standard deviation of the measurement.

Normalizing the emissions, by dividing each emission value by that associated with the slowest forward travel speed for both sites, and including the available $PM_{2.5}$ data (also normalized to the slowest forward travel speed), shows that the emissions of either size class of particulate matter, from both sites, scale similarly with forward travel speed of the aircraft (Fig. 8).

4.2. Surface shear stress relationships

That the emission of dust is related to the forward travel speed of the aircraft suggests that the force driving the emissions is related to the shear stress created by the rotor downwash, similar to wind-generated dust emissions (Shao, 2000). The Irwin sensor data provide a means to examine the near surface shear stress generated by the outflow of air from the rotor-blade. The Irwin sensors are calibrated to measure the delta pressure (Pa) difference between the surface and that measured at a height above that surface, but

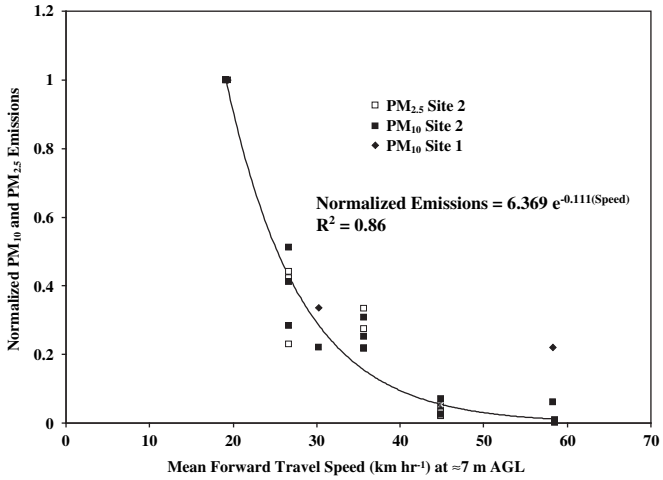

Fig. 8. Normalized emissions of PM_{10} and $PM_{2.5}$ as a function of mean forward travel speed for Sites 1 and 2, YPG.

very close to the surface. Typically, and in this case as well, that height is 1.651 mm.

According to Irwin (1980), the delta pressure can be related to a shear stress (τ, N m^{-2}) using the following calibration relationship:

$$\frac{u_\tau h}{\nu} = 8.0 + 0.193\left(\frac{\Delta p h^2}{\rho \nu^2}\right)^{0.453} \quad (4)$$

where: u_τ is skin friction velocity (m s^{-1}, note $u_\tau = (p_{air} \times \tau)^{0.5}$), h is the height above the surface of the second pressure measurement (i.e., 1.651 mm), ν is kinematic viscosity (m^2 s^{-1}), p is pressure (Pa), and ρ is fluid density (kg m^{-3}).

An example of the delta pressure data obtained from the two of the four Irwin sensors is shown in Fig. 9 (the closest and furthest sensors from the flight line) for a helicopter pass at the forward travel speed of 15 km h^{-1} at site 2. These data show that the Irwin closest to the flight line (10 m from the centerline) experiences higher pressures than the one farthest away and the peak pressures occur later in time with increasing distance from the flight line, representing the flow of air outward from the source. By aggregating the pressure data and converting it to a shear stress the relationship between aircraft forward speed and shear stress as a function of distance from the Irwin sensors can be examined. It should be noted that the calibration i.e., Eq. (3) developed by Irwin (1980) was for a smooth surface and the test surfaces at YPG were neither physically nor aerodynamically smooth, so the absolute magnitude of the shear stress measurements have an unknown error associated with them. The data they provide, however, is still valuable and gives information on the pattern of shear stress created by the rotor-blade downwash that creates the dust emissions.

The effect of forward travel speed on surface shear stress is shown in Fig. 10 in which the normalized mean peak shear stress at each Irwin sensor location is plotted against mean forward travel speed. The peak shear stress at each measurement position was normalized by dividing by the mean peak shear stress for the 15 km h^{-1} speed. This relationship is shown in Fig. 10 and it reveals that the shear stress changes proportionally the same amount at each measurement location for an incremental change in forward travel speed. At each of the Irwin sensor locations there is an ≈0.12% decrease in mean peak shear stress for every 10 km h^{-1} increase in forward travel speed.

The Irwin sensor data can also be used to evaluate how the shear stress distribution changes as a function of distance from the flight line. The decrease in mean peak shear stress as a function of distance from the flight line and for all average test speeds is shown for sites 1 and 2 in Fig. 11. In Fig. 11 these data are normalized by dividing the measured mean peak shear stress at each instrument position by that measured at the first Irwin sensor (i.e., 10 m from the flight line center), which collapses the data for each travel speed and each site.

4.3. Take-off and landing

At site 1 the emissions from three landings and four take-offs in close proximity to each other were measured. The emission flux expressed as kg of PM_{10} passing the flux plane for each event (landing or take-off) is shown in Fig. 12a. The average take-off and landing emission fluxes are shown in Fig. 12b. These types of emissions are basically from a point on the surface and are lower in total mass emissions than the low-level flight tests. Based on the average emission values shown in Fig. 12b, a take-off produced approximately 0.5 kg of PM_{10} and a landing approximately 1 kg, which likely reflects the time associated with each maneuver as a take-off occurs more quickly than a landing.

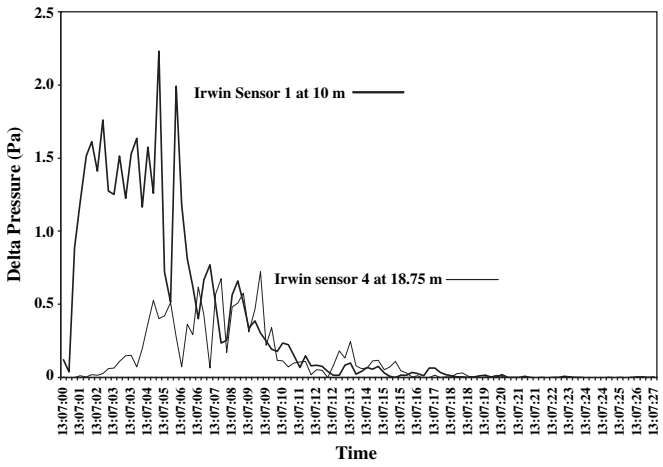

Fig. 9. Time series of delta pressure (Pa) measured with the Irwin sensors that are placed in increasing distance normal to the flight line of the aircraft beginning 10 m from the edge of the rotor-blade. For clarity only the sensors closets to and furthest from the flight line are presented.

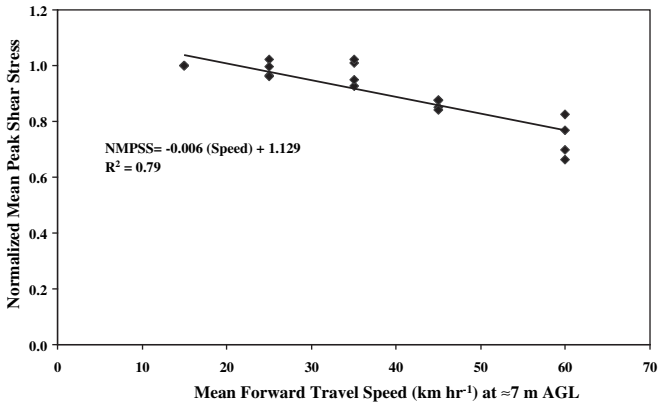

Fig. 10. The relationship between normalized mean peak pressure and mean forward travel speed for Sites 1 and 2 combined showing that peak shear stress decreases at the same increment at each measurement location over the ≈19 m measurement length as aircraft speed increases.

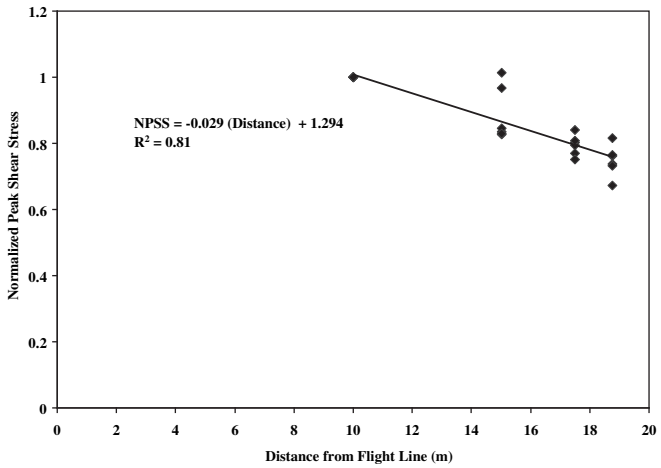

Fig. 11. The relationship between normalized mean peak pressure and distance from the centerline of the aircraft flight line (i.e., centerline is 0 m) for Sites 1 and 2 combined showing that peak shear stress decreases linearly with increasing distance over the 19 m measurement length independent of aircraft speed.

4.4. PI-SWERL emission potential measurements

At site 1, the transect of PI-SWERL measurements produced shear stresses ranging from 0.06 N m^{-2} to 0.77 N m^{-2} with the highest shear stress generating PM_{10} dust emissions that exceeded the limit (150 mg m^{-3}) of the dust monitor incorporated into the instrument. The variability between tests is considerable with the standard deviation of the tests (pre- and post-helicopter passes) exceeding the geometric mean of the tests at each shear stress interval. The range of PM_{10} emissions can be expressed by the geometric mean of all of the tests combined for shear stresses of 0.06 N m^{-2}, 0.18 N m^{-2}, 0.36 N m^{-2}, 0.55 N m^{-2}, and 0.77 N m^{-2}, which were 0.011 mg m^{-2} s^{-1}, 0.060 mg m^{-2} s^{-1}, 0.346 mg m^{-2} s^{-1}, 2.168 mg m^{-2} s^{-1}, 4.069 mg m^{-2} s^{-1}, respectively. The difference before and after the helicopter passes in dust emissions was not statistically significant, but the emissions were higher on average for the same shear stress for the PI-SWERL tests post-helicopter passes (e.g., for a shear stress of 0.77 N m^{-2} the PM_{10} emissions were 2.86 mg m^{-2} s^{-1} and 6.87 mg m^{-2} s^{-1} for the pre- and post-helicopter passes, respectively).

The range of PM_{10} emissions estimated using PI-SWERL for site 2 expressed by the geometric mean of all of the tests combined for shear stresses of 0.06 N m^{-2}, 0.18 N m^{-2}, 0.36 N m^{-2}, and 0.55 N m^{-2}, were 0.062 mg m^{-2} s^{-1}, 0.167 mg m^{-2} s^{-1}, 3.244 mg m^{-2} s^{-1}, and 21.635 mg m^{-2} s^{-1}, respectively. The variability in emissions amongst the tests at this site is relatively large resulting in a large standard deviation of the measured emission flux. On average, however, the emissions from site 2 were an order of magnitude larger than at site 1 for the same shear stresses. The surfaces at site 2 were very emissive and exhibited PM_{10} emissions beyond those measured at typical natural southwest desert surfaces measured with the PI-SWERL (Sweeney et al., 2008).

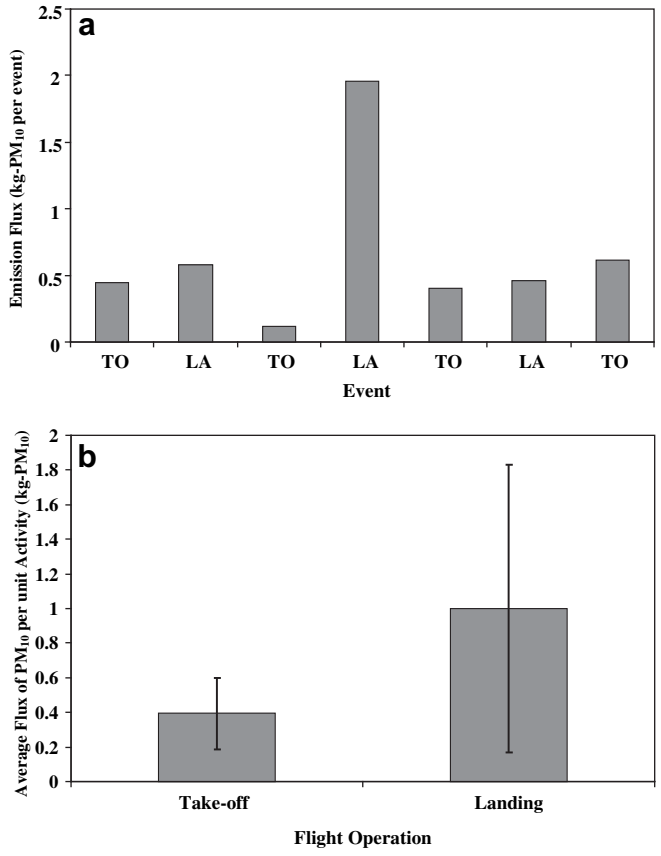

Fig. 12. (a) The emission flux of PM_{10} for each take-off (TO) and landing (LA) event at Site 1. (b) The average emission flux of PM_{10} for each type of flight operation measured at Site 1.

5. Discussion

As Fig. 7 shows there is a clear reduction in PM emissions as aircraft speed increases. A two-part mechanism can be proposed that explains this relationship. First, as the helicopter's forward speed increases its residence time over any location on the surface diminishes, so the time the downward rotor-generated flow is acting upon that surface also decreases. This reduces the duration that the shear stress is applied at any one point on the flight path so the duration during which emissions of dust could occur also decreases.

Second, as mentioned previously, changes in forward travel speed are controlled only by the rotor-blade positional characteristics while the rate of revolution of the helicopter rotor is essentially held constant. As the helicopter increases its forward speed, the rotor-blades change their pitch over the 360° rotation. This change in pitch alters the strength and distribution of the shear stresses created by the downward directed air flow from the rotor, which will also affect the dust emission process. This is clearly seen in the Irwin sensor data (i.e., Fig. 10), which show that mean peak shear stress decreases with increasing forward travel speed. The relative change in the shear stress at locations perpendicular to the flight line (outside of the area defined by the rotor diameter) scale predictably with travel speed.

Another potentially critical component affecting dust emissions may be the flow regime that is created under the aircraft, which will be dictated to a large degree by the ambient wind speed and the rotor-blade pitch (forward travel speed). Peak shear stresses at the surface are likely to be lower as higher ambient wind speeds force the advance ratio towards a trailing sweep or ground vortex regime. The data collected do not allow for an evaluation of the potential influence of flow regime on dust emissions.

Based on these observations, for similarly configured aircraft (i.e., one main rotor and one tail rotor), several physical characteristics of the aircraft are likely to have a direct bearing on the strength of the dust emissions. These are the weight of the aircraft, the length of the rotor-blades, and possibly the number of rotor-blades. Weight is critical because it defines how much force is

needed to keep the aircraft aloft. The length of the rotor-blades and their number will also be important as they effect the force per unit area felt on the ground surface. With the present data set it is not possible to evaluate how different rotor-blade and weight configurations may affect dust emissions.

Cowherd (2007) however, presents data for dust concentrations measured in plumes generated by five different rotary-winged aircraft (UH-1, CH-46, HH-60, CH-53, and MH-53) at two different positions downwind (17.5 m and 35 m from the rotor edge) of low-level flight passes and at two different heights (0.5 m and 1.4 m), which can be used to demonstrate the effect of aircraft weight and rotor-blade length on dust emissions. Normalizing Cowherd's (2007) data (refer to Table 11 in Cowherd, 2007) by dividing each disk loading value by the lowest value (for the UH-1) and normalizing each concentration by dividing by the lowest measured value collapse these data and produces the relationship shown in Fig. 13. This relationship (Fig. 13) shows normalized concentration increases as a power function of normalized disk loading, which suggests that the dust flux should also increase as a power function of disk loading.

A comparison of emissions of PM_{10} from the rotary-winged test aircraft and the military wheeled vehicles tested by Gillies et al. (2005) (i.e., HUMMWV, LMTV, 5-ton, and HEMMT) for the speed range of 15 km h^{-1} to 60 km h^{-1} is shown in Fig. 14. As Fig. 14 shows, the emissions of PM_{10} dust from low-flying rotary-winged aircraft only approach the levels associated with wheeled vehicles when they travel slowly over surfaces that have similar emission potentials to the test sites at YPG.

Emissions of PM_{10} dust calculated from available emission factor relationships for wheeled military vehicles (Gillies et al., 2005) would exceed those generated by this type of helicopter, for essentially all normal operating speeds for both types of vehicles, for site 1. For site 2, the aircraft-generated PM_{10} emissions would exceed those of the lowest weight wheeled vehicle for travel speeds less than ≈23 km h^{-1}. For the two heaviest wheeled vehicles (HEMMT and 5-ton) the rotary-winged aircraft will emit more PM_{10} per kilometer of travel when both vehicle speeds are less than ≈12 km h^{-1}. It should be noted that the emission factor relationship with speed for the rotary-winged aircraft is an underestimation, as the total plume dimensions were not captured by the instrument array. Increasing the emissions by one standard deviation above the mean (approximately doubling the values), emissions of PM_{10} dust per vehicle kilometer travelled from the rotary-winged aircraft would be higher than those of the heaviest and lightest wheeled vehicles (i.e., HEMMET and HUMVEE) if the aircraft travelled at speeds less than ≈16 km h^{-1} and ≈26 km h^{-1}, respectively at site 2. It is unlikely that the sampling system underestimated the emissions by a factor greater than two, as observed plume heights did not loft much higher than the tops of the towers. We are confident that these acquired data show that emissions from low-flying rotary-winged aircraft of the type typified by the test model are representative and can be used to estimate contributions to regional PM levels using an inventory approach. It must also be noted that the aircraft in this study flew at the minimum height above ground level that the pilots were allowed to fly due to safety restrictions. It is expected that emissions would decrease with increasing aircraft altitude, for the same forward travel speed, as the force of the rotor downwash would be spread over a larger area on the ground. In addition, the strength of the downwash would lessen as the turbulence in the flow decayed due to the greater amount of time that viscous forces would aid in dissipation of the wake turbulence.

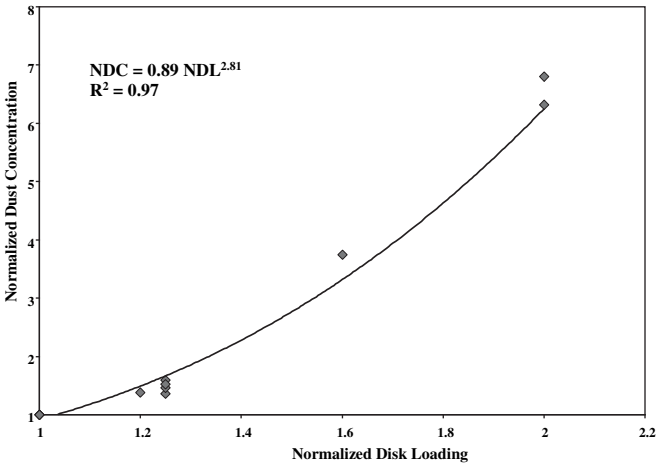

Fig. 13. Normalized dust concentration as a function of normalized disk loading showing how aircraft weight and the area swept by the rotor-blades affect the strength of the dust concentrations in the plume (after Cowherd, 2007).

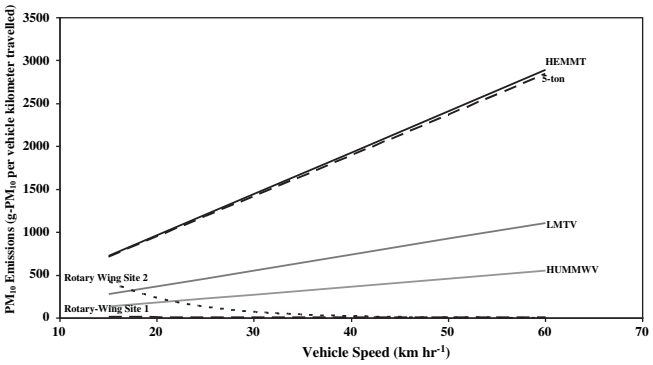

Fig. 14. Comparison of emissions of PM_{10} as a function of vehicle speed for the rotary-winged aircraft and light and heavy wheeled military vehicles. Wheeled vehicle emission factors are from Gillies et al. (2005).

In view of this, it is also likely that the actual contributions of dust emissions from low-level flight of rotary-winged aircraft are not a critical component of the total emission contributions of PM_{10} or $PM_{2.5}$ that originate from DoD testing and training activities. The overall travel distances that rotary-winged aircraft cover while in low-level flight are probably orders of magnitude smaller than those of wheeled vehicles traveling on unpaved surfaces. Two factors support this assumption: the first is the number of wheeled vehicles used by the DoD is far greater than the number of helicopters, and the second is low-level flights do not comprise a major component of flight training. Even a take-off or landing, which produce brief emission bursts, likely does not produce significant contributions to regional PM levels as these maneuvers are not undertaken often on emissive surfaces for safety reasons (e.g., visibility, mechanical failure).

6. Conclusions

This work provides data on the strength of dust emissions created by low-level rotary-winged aircraft, which to the best of our knowledge, has not been reported elsewhere in the peer-reviewed literature. For rotary-winged aircraft flying under the conditions prescribed by the testing, emission rates of PM_{10} for each meter of forward travel were observed to scale primarily as a function of forward travel speed, decreasing roughly exponentially as travel speed increases. Based on surface shear stress measurements for each increase in speed there is a decrease in the peak shear stress in a zone extending from ≈19 m beyond the edge of the main rotor and

the data from these measurement indicate that the magnitude of the shear stress decays as a function of distance from near the rotor edge. This decay in shear stress as a function of distance is likely exponential, but this was not observed due to the relatively short ($\approx$19 m) measurement distance. Speed affects dust emissions in two ways: 1) as speed increases, peak shear stress at the surface was observed to decline proportionally, and 2) as the helicopter's forward speed increases its residence time over any location on the surface diminishes, so the time the downward rotor-generated flow is acting upon that surface also decreases. Based on data available in Cowherd (2007) it was also demonstrated that emissions likely scale as a function of the weight of the aircraft and the area defined by the sweep of its rotor-blade as well as its speed. Altitude of the aircraft will also affect emissions, but this was not quantified in this study.

Based on the measured emission rates for the test aircraft, it is fairly certain that dust emissions from rotary-winged aircraft do not constitute a significant source of PM_{10} and $PM_{2.5}$ originating from testing and training on U.S. military installations. Given that wheeled and tracked vehicles produce more emissions per unit distance travelled than rotary-winged aircraft for speeds that exceed 15 km h^{-1}, it is suggested here that controlling or mitigating emissions from wheeled and tracked vehicles offers a greater opportunity to reduce dust loading associated with testing and training involving these types of vehicles than rotary-winged aircraft.

The PI-SWERL emissions measurements showed that site 2 was potentially more emissive than site 1, which was reflected in the tower-based measurements of the aircraft-generated emissions. Both measurements were approximately an order of magnitude different between the sites. It will require a larger data set to evaluate if these two measurement methods scale similarly, which if proved would allow PI-SWERL to be used as an economical means for evaluating emission potential for rotary-winged aircraft.

Acknowledgments

We would like to acknowledge the great support offered in the field by YPG personnel, in particular the flight crews and ground crew (Mike Jonez and Co.). We are also appreciative of the support of Graham Stullenbarger and Wayne Lucas of the Natural Environments Test Office, YPG for logistical and financial support. We would also like to thank the SERDP Sustainable Infrastructure program for their continued support of this project (SI-1399). We also thank the reviewer who directed us to the Cowherd (2007) report.

References

Brown, R., Whitehouse, G., 2004. Modelling rotor wakes in ground effect. Journal of the American Helicopter Society 49 (3), 238–249.

Chow, J.C., Watson, J.G., Houck, J.E., Pritchett, L.C., Rogers, C.F., Frazier, C.A., Egami, R.T., Ball, B.M., 1994. A laboratory resuspension chamber to measure fugitive dust size distributions and chemical compositions. Atmospheric Environment 28 (21), 3463–3481.

Cowherd, C., 2007. Sandblaster 2 Support of See-Through Technologies for Particulate Brownout. Task 5 Final Technical Report, MRI Project No. 110565, 42 p.

Curtiss, H., Erdman, W., Sun, M., 1987. Ground effect aerodynamics. Vertica 11 (1/2), 29–42.

Curtiss, H.C., Sun, M., Putman, W.F., Hanker, E.J., 1984. Rotor aerodynamics in ground effect at low advance ratios. Journal of the American Helicopter Society 29 (1), 48–55.

Etyemezian, V., Nikolich, G., Ahonen, S., Pitchford, M., Sweeney, M., Gillies, J., Kuhns, H.D., 2007. The Portable In-Situ Wind Erosion Laboratory (PI-SWERL): a new method to measure PM_{10} windblown dust properties and potential for emissions. Atmospheric Environment 41, 3789–3796.

Ganesh, B., Komerath, N., 2004a. Unsteady aerodynamics of rotorcraft in ground effect. In: Proc. of the 34th AIAA Fluid Dynamics Conf., 28 Jun.–1 Jul. 2004, Portland, Oregon AIAA-2004-2431.

Ganesh, B., Komerath, N., 2004b. Unsteady aerodynamics of rotorcraft in ground effect. In: Proc. of the 22nd Applied Aerodynamics Conf., 16–19 Aug. 2004, Providence, Rhode Island, AIAA-2004-5287.

Ganesh, B., and Komerath, N., 2006. Study of ground vortex structure of rotorcraft in ground effect at low advance ratios. In: Proc of the 24th Applied Aerodynamics Conf., 5–8 Jun. 2006, San Francisco, CA, AIAA-2006-3475.

Gillies, J.A., Berkofsky, L.B., 2004. Eolian suspension above the saltation layer, the concentration profile. Journal of Sedimentary Research 74, 176–183.

Gillies, J.A., Etyemezian, V., Kuhns, H., Nikolic, D., Gillette, D.A., 2005. Effect of vehicle characteristics on unpaved road dust emissions. Atmospheric Environment 39, 2341–2347.

Gillies, J.A., Kuhns, H.D., Engelbrecht, J.P., Uppapalli, S., Etyemezian, V., Nikolich, G., 2007a. Particulate emissions from U.S. Department of defense artillery backblast testing. Journal of the Air & Waste Management Association 57, 551–560.

Gillies, J.A., Nickling, W.G., King, J., 2007b. Shear stress partitioning in large patches of roughness in the atmospheric inertial sublayer. Boundary-Layer Meteorology 122, 367–396.

Gillies, J.A., Nickling, W.G., King, J., 2006. Aeolian sediment transport through large patches of roughness in the atmospheric inertial sublayer. Journal of Geophysical Research – Earth Surface 111 doi:10.1029/2005JF000434.

Gillies, J.A., Watson, J.G., Rogers, C.F., DuBois, D., Chow, J.C., 1999. Long-term efficiencies of dust suppressants to reduce PM10 emissions from unpaved roads. Journal of the Air & Waste Management Association 49, 3–16.

Goossens, D., Buck, B., 2009. Dust dynamics in off-road vehicle trails: measurements on 16 arid soil types, Nevada, USA. Journal of Environmental Management 90 (11), 3458–3469,. doi:10.1016/j.jenvman.2009.05.031.

Irwin, H.P.A.H., 1980. A simple omnidirectional sensor for wind tunnel studies of pedestrian level winds. Journal of Wind Engineering and Industrial Aerodynamics 7, 219–239.

Kavouras, I.G., Etyemezian, V., Nikolich, G., Young, M., Gillies, J., Shafer, D., 2009. A new technique for characterizing the efficacy of fugitive dust suppressants. Journal of the Air & Waste Management Association 59, 603–612. doi:10.3155-1047-3289.59.5.603.

King, J., Etyemezian, V., Sweeney, M., Buck, B., Nikolich, G. Dust emission variability at the Salton Sea, California, USA. Geomorphology, submitted for publication.

Kuhns, H., Gillies, J.A., Etyemezian, V., Nikolich, G., King, J., Zhu, Uppapalli, S., Engelbrecht, J. and Kohl, S. Particulate matter emissions from wheeled and tracked vehicles operating on unpaved roads. Aerosol Science and Technology, in press.

McAlpine, J.D., Koračin, D., Gillies, J.A., Boyle, D., McDonald E. Rotorcraft ground-effect wake observations from a full-scale experiment over desert terrain. Journal of the American Helicopter Society, submitted for publication.

Moosmüller, H., Arnott, W.P., Rogers, C.F., Bowen, J.L., Gillies, J.A., Pierson, W.R., Collins, J.F., Durbin, T.D., Norbeck, J.M., 2001a. Time resolved characterization of diesel particulate emissions: 1. Instruments for particle mass measurements. Environmental Science & Technology 35, 781–787.

Moosmüller, H., Arnott, W.P., Rogers, C.F., Bowen, J.L., Gillies, J.A., Pierson, W.R., Collins, J.F., Durbin, T.D., Norbeck, J.M., 2001b. Time resolved characterization of diesel particulate emissions: 2. Instruments for elemental and organic carbon measurements. Environmental Science & Technology 35, 1935–1942.

Moosmüller, H., Varma, R., Arnott, W.P., Kuhns, H.D., Etyemezian, V., Gillies, J.A., 2005. Scattering cross section emission factors for visibility and radiative transfer applications: military vehicles traveling on unpaved roads. Journal of the Air and Waste Management Association 55, 1743–1750.

Shao, Y., 2000. Physics and Modelling of Wind Erosion. Kluwer Academic Publishers, Dordrecht, pp. 393.

Sweeney, M., Etyemezian, V., Macpherson, T., Nickling, W.G., Gillies, J., Nikolich, G., McDonald, E., 2008. Comparison of PI-SWERL with dust emission measurements from a straight-line field wind tunnel. Journal of Geophysical Research - Earth Surface 113 F01012, doi:10.1029/2007JF000830.

U.S. Environmental Protection Agency, 1996. Compilation of Air Pollutant Emission Factors. In: Stationary Point and Area Sources, vol. 1. US EPA Office of Air and Radiation, Office of Air Quality Planning and Standards, RTP, NC.